J|A|C|S
ARTICLES
Published on Web 11/25/2004

Structural, Volumetric, and Thermodynamic Characterization of a Micellar Sphere-to-Rod Transition

Heiko Heerklotz,*,† Alekos Tsamaloukas,† Katarzyna Kita-Tokarczyk,‡ Pavel Strunz,§ and Thomas Gutberlet§

Contribution from the Biozentrum, University of Basel, Klingelbergstrasse 70, CH-4056 Basel, Switzerland, Department of Chemistry, University of Basel, Klingelbergstrasse 80, CH-4056 Basel, Switzerland, and Paul Scherrer Institute, CH-5232 Villigen PSI, Switzerland

Received July 26, 2004; E-mail: heiko.heerklotz@unibas.ch

Abstract: The thermotropic sphere-to-rod transition of nonionic surfactants was characterized in terms of a large set of parameters: the transition temperature and width, the partial volume, coefficient of thermal volume expansion, enthalpy, isobaric heat capacity, and structural parameters, such as radius of gyration and hydrodynamic radius. Data were recorded as a function of concentration of surfactants in H_2O and in D_2O. To this end, pressure perturbation calorimetry (PPC), small angle neutron scattering (SANS), dynamic light scattering (DLS), differential scanning calorimetry (DSC), and isothermal titration calorimetry (ITC) were applied in a study of aqueous solutions containing myristyl, tridecyl, and lauryl maltoside and heptaethyleneglycoltetradecyl ether ($C_{14}EO_7$). Small changes in the thermodynamic and volumetric parameters (e.g., the partial volume change is $\sim$+2‰) are discussed in detail as the result of three effects governing the transition. (i) Reduction of the water accessible hydrophobic surface area (ASA_{ap}) drives the transition. (ii) Shrinking in headgroup size by thermal dehydration triggers the transition. (iii) Hypothesized gradual ordering of the chains may control the effect of chain length on the transition.

Introduction

In this paper, we present a comprehensive description including the first data on the volumetric properties of micellar sphere-to-rod transitions. Volume changes were measured by means of pressure perturbation calorimetry (PPC), a method which has only recently been introduced and applied to study proteins,[1−3] polymers,[4] and phospholipids.[5,6] A criticism of the technique[7] was shown to be irrelevant.[8,9] PPC is based on the measurement of the heat response of a solution to a small pressure jump of 5 bar and yields the temperature-dependent coefficient of thermal expansion and, in turn, the volume change accompanying a thermotropic transition of solutes or colloids.

The transition of spherical surfactant micelles in solution to a cylindrical geometry was already described by Luzzati[10] in 1964 and has been thoroughly studied since then by light scattering,[11,12] SANS,[13−16] and electron microscopy.[17] A particular issue of scattering data has been to distinguish between the continuous rodlike structures and the effects of critical fluctuations and attractive interactions between small micelles.[16,18] The terms cylindrical, rodlike, threadlike, or polymer-like micelles describe the same general geometry but may emphasize different properties with respect to length, flexibility, or branching; we will however use the term rodlike for any micelle with a locally cylindrical structure, regardless of these specific properties.

Most sphere-to-rod transitions can be explained in terms of a simple but useful *packing model* described by Israelachvili,[19] which is based on three criteria: (i) the surface-to-volume ratio of the aggregates in relation to the molecular dimensions, (ii) the fact that the radius of the core cannot exceed the maximum projected chain length, and (iii) that smaller aggregates are entropically favored over larger ones. First, the surface-to-volume ratio of the hydrophobic core of the aggregate, A/V, agrees with the ratio of the surface increment covered by the

† Biozentrum.
‡ Department of Chemistry.
§ Paul Scherrer Institute.

(1) Lin, L. N.; Brandts, J. F.; Brandts, J. M.; Plotnikov, V. *Anal. Biochem.* **2002**, *302*, 144−160.
(2) Sasisanker, P.; Oleinikova, A.; Weingartner, H.; Ravindra, R.; Winter, R. *Phys. Chem. Chem. Phys.* **2004**, *6*, 1899−1905.
(3) Ravindra, R.; Winter, R. *ChemPhysChem* **2004**, *5*, 566−571.
(4) Kujawa, P.; Winnik, F. M. *Macromolecules* **2001**, *34*, 4130−4135.
(5) Wang, S. L.; Epand, R. M. *Chem. Phys. Lipids* **2004**, *129*, 21−30.
(6) Heerklotz, H.; Seelig, J. *Biophys. J.* **2002**, *82*, 1445−1452.
(7) Randzio, S. L. *Thermochim. Acta* **2003**, *398*, 75−80.
(8) Heerklotz, H. *J. Phys.: Condens. Matter* **2004**, *16*, R441−467.
(9) Brandts, J.; Lin, L. *Thermochim. Acta* **2004**, *414*, 95−100.
(10) Reiss-Husson, F.; Luzzati, V. *J. Phys. Chem.* **1964**, *68*, 3504−3511.
(11) Cirkel, P. A.; Koper, G. J. M. *Langmuir* **1998**, *14*, 7095−7103.
(12) von Berlepsch, H.; Dautzenberg, H.; Rother, G.; Jaeger, J. *Langmuir* **1996**, *12*, 3613−3625.
(13) He, L. Z.; Garamus, V. M.; Funari, S. S.; Malfois, M.; Willumeit, R.; Niemeyer, B. *J. Phys. Chem. B* **2002**, *106*, 7596−7604.
(14) He, L. Z.; Garamus, V.; Niemeyer, B.; Helmholz, H.; Willumeit, R. *J. Mol. Liq.* **2000**, *89*, 239−248.
(15) Stradner, A.; Glatter, O.; Schurtenberger, P. *Langmuir* **2000**, *16*, 5354−5364.
(16) Glatter, O.; Fritz, G.; Lindner, H.; Brunner-Popela, J.; Mittelbach, R.; Strey, R.; Egelhaaf, S. U. *Langmuir* **2000**, *16*, 8692−8701.
(17) Bernheim-Groswasser, A.; Wachtel, E.; Talmon, Y. *Langmuir* **2000**, *16*, 4131−4140.
(18) Lindman, B.; Wennerstrom, H. *J. Phys. Chem.* **1991**, *95*, 6053−6054.
(19) Israelachvili, J. N. *Intermolecular and Surface Forces*, 2nd ed.; Academic Press: London, 1991.

10.1021/ja045525w CCC: $27.50

headgroup, a_0, to the partial volume of the hydrophobic tail, v_{chain} (i.e., $A/V = a_0/v_{chain}$). The optimum area per headgroup, a_0, depends not only on steric properties but also on electrostatic interactions, hydration, and other forces governing the packing density of the headgroups. It is straightforward to verify that the surface-to-volume ratio, A/V, is inversely proportional to the radius (or half bilayer thickness), R, amounting to $1/R$ for a lamella, $2/R$ for a cylinder, and $3/R$ for a sphere. The second criterion requires that a tail must be able to reach the center of the micelle so that the radius R is limited by the maximum projected length of the tail, l_{max}: $R \leq l_{max}$. Hence, spheres can be formed for a so-called packing parameter $\gamma \equiv v_{chain}/(a_0 l_{max}) \leq {}^1/_3$, cylinders for $\gamma \leq {}^1/_2$, and bilayer vesicles for $\gamma \leq 1$. Finally, the model assumes that more, smaller particles are entropically favored over fewer, larger ones (e.g., spheres over rods).

This concept explains why sphere-to-rod transitions of micelles can proceed (i) upon addition of a hydrophobic compound or a cosurfactant with large v_{chain} and small a_0, such as alcohols and diacyl phospholipids,[15,20−22] and (ii) by reducing a_0 of ionic surfactants by addition of salt[12] or counterionic surfactants.[23] For nonionics, it may be induced (iii) with increasing temperature since thermal dehydration diminishes a_0,[24,25] but for ionic surfactants, it was observed (iv) with decreasing temperature.[26] Being a growth or association phenomenon, the transition can also proceed (v) with increasing concentration.[27−29]

Grell et al.[24] established thermotropic sphere-to-rod transitions for $C_{14}EO_6$ and $C_{16}EO_8$ by SANS and measured the *enthalpy change* (∼+2 kJ/mol) by differential scanning calorimetry (DSC). DSC scans of lipid−surfactant mixtures showed endotherms related to micellar growth or association below the cloud point.[30] Isothermal titration calorimetry (ITC) in which the lipid POPC was injected into micelles of $C_{12}EO_n$ at room temperature revealed transitions at a lipid mole fraction of 12% for $C_{12}EO_7$ [31] and of 24% for $C_{12}EO_8$ [21] that were accompanied by an increase in excess enthalpy (∼1−2 kJ/mol)[31] and also identified as sphere-to-rod transitions by SANS.[22] Since ionic surfactants, such as SDS, exhibit a sphere-to-rod transition with decreasing temperature,[18] the enthalpy changes are exothermic.[26,32]

Volumetric data on the sphere-to-rod transition are extremely rare, most likely since the accompanying changes in the absolute volume or density of the solution are very small. Gonzalez-Perez et al.[33] found slight discontinuities in the partial molar volume of myristoyldimethylbenzylammonium chloride as a function of concentration, suggesting a volume change of ∼+0.45 mL/mol at 25 °C and decreasing with increasing temperature. They interpreted this finding in terms of a partial dehydration of headgroups and counterions (due to stronger binding to the surfactant). Application of 2.5 kbar to solutions of flexible, branched rodlike micelles of $C_{12}E_5$ did not induce a transition to spheres, as one might expect if the volume expands at a sphere-to-rod transition, but a freezing of the hydrophobic core leading to hexagonally packed, stiff, unbranched cylinders.[34]

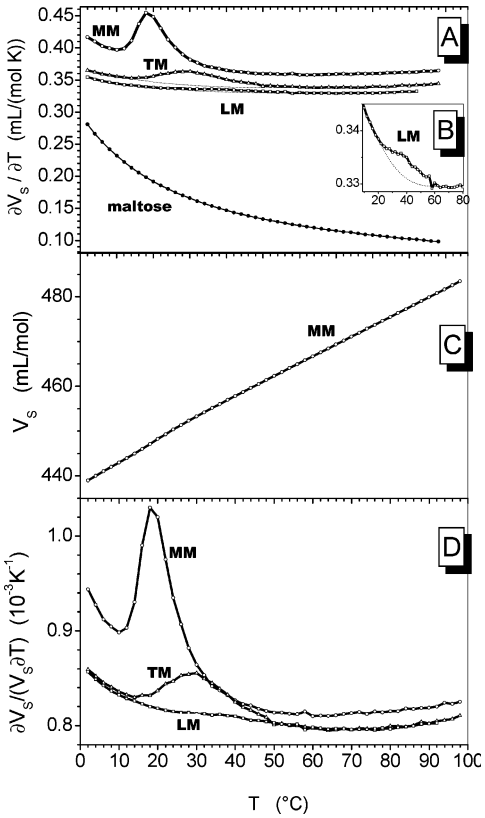

Figure 1. (A) PPC curves of lauryl (LM), tridecyl (TM), and myristyl (MM) maltoside and maltose in water (100 mM), showing the thermal expansion of the partial molar volume of the surfactants, $\partial V_S/\partial T$, as a function of temperature, T. (B) Zoomed reproduction of the curve of LM shown in A. (C) Partial molar volume of MM, $V_S(T)$, obtained by integration of the PPC curve using a value of $V_S(20\ °C) = 448$ mL/mol for the integration constant (cf. Experimental Section in the Supporting Information). Note that the transition is hardly visible in the integral curve. (D) Temperature-dependent coefficient of thermal expansion, $\alpha = \partial V_S/(V_S\partial T)$, corresponding to the curves shown in panel A.

Results

PPC. Figure 1A shows curves of the molar expansivity, for example, the change in partial molar volume of the solute, V_S, with temperature, T, of micellar dispersions of alkyl maltosides in water. Pronounced peaks are observed, in particular, for myristyl maltoside (MM) and tridecyl maltoside (TM), representing thermal transitions that are accompanied by an increase in volume. The peaks become larger, narrower, and shifted to a lower temperature with increasing length of the alkyl chain.

Integration of the PPC curve from an arbitrarily defined baseline (cf. dotted lines in the figure) yields the volume change of the transition, ΔV_S, which amounts to ∼1 mL/mol for MM

(20) Walter, A.; Vinson, P. K.; Kaplun, A.; Talmon, Y. *Biophys. J.* **1991**, *60*, 1315−1325.
(21) Heerklotz, H.; Lantzsch, G.; Binder, H.; Klose, G.; Blume, A. *J. Phys. Chem.* **1996**, *100*, 6764−6774.
(22) Gutberlet, T.; Kiselev, M.; Heerklotz, H.; Klose, G. *Physica B* **2000**, *276*, 381−383.
(23) Raghavan, S. R.; Fritz, G.; Kaler, E. W. *Langmuir* **2002**, *18*, 3797−3803.
(24) Grell, E.; Lewitzki, E.; Schneider, R.; Ilgenfritz, G.; Grillo, I.; von Raumer, M. *J. Therm. Anal.* **2002**, *68*, 469−478.
(25) Briganti, G.; Bonincontro, A. *J. Non-Cryst. Solids* **1998**, *235*, 704−708.
(26) Mazer, N. A.; Olofsson, G. *J. Phys. Chem.* **1982**, *86*, 4584−4593.
(27) Miura, M.; Kodama, M. *Bull. Chem. Soc. Jpn.* **1972**, *45*, 428−431.
(28) May, S.; Ben-Shaul, A. *J. Phys. Chem. B* **2001**, *105*, 630−640.
(29) Al-Anber, Z. A.; Avalos, J. B. I.; Floriano, M. A.; Mackie, A. D. *J. Chem. Phys.* **2003**, *118*, 3816−3826.
(30) Kresheck, G. C.; Mihelich, J. *Chem. Phys. Lipids* **2003**, *123*, 45−62.
(31) Heerklotz, H. H.; Binder, H.; Schmiedel, H. *J. Phys. Chem. B* **1998**, *102*, 5363−5368.
(32) Gu, G. X.; Yan, H. K.; Chen, W. H.; Wang, W. Q. *J. Colloid Interface Sci.* **1996**, *178*, 614−619.
(33) Gonzalez-Perez, A.; Czapkiewicz, J.; Del Castillo, J. L.; Rodriguez, J. R. *Colloid Surf., A* **2001**, *193*, 129−137.
(34) Bossev, D. P.; Kline, S. R.; Israelachvili, J. N.; Paulaitis, M. E. *Langmuir* **2001**, *17*, 7728−7731.

Table 1. Results of PPC and DSC Experiments[a]

		C_S (mM)	T_{sr} (°C)	ΔT_{sr} (K)	ΔV_S (mL/mol)	$\Delta V_S/V_S$ (‰)	ΔH (kJ/mol)	c.u.
LM	H_2O	100	40	24	0.1	0.2		
TM	H_2O	100	30	20	0.5	1.1		
	H_2O	37	37	23	0.3	0.7	0.2	600
	D_2O	37	30	20	0.3	0.7	0.2	800
MM	H_2O	300	13.5	7	1.1	2.5	0.6	600
		100	19.4	9	1.0	2.2	0.6	500
		37	23.1	11	1.0	2.2	0.6	300
		10	30.0	16	1.0	2.2		
	D_2O	37	19.6	8	0.9	2.0	0.5	600
$C_{14}E_7$	H_2O	100	18.7	9	0.7	1.5	1.9	140
	D_2O	100	17.4	8			1.5	230

[a] Estimated errors are typically ±1, at the most ±2, of the last digit. T_{sr} and ΔT_{sr} are obtained consistently from DSC (high resolution in T) and PPC (low resolution) curves.

(cf. Table 1). The temperature at the maximum of $\partial V_S/\partial T$, T_{sr}, and the full width at half-height, ΔT_{sr}, are listed in Table 1. The PPC curve of lauryl maltoside (LM) shows only a very weak discontinuity (enlarged in Figure 1B). The expansivity curve for maltose is shown for comparison.

Figure 1C shows the partial molar volume, V_S, of MM as a function of temperature, which was derived by integrating the PPC curve (Figure 1A) with an integration constant chosen to reach a specific volume of 0.83 mL/g at 20 °C (cf. Experimental Section in the Supporting Information). It is noteworthy that PPC is far more sensitive to reveal the transition than methods determining the absolute volume or density since a slight (~10%) increase of the slope of $V_S(T)$ in a certain temperature range (Figure 1C) gives rise to a sharp peak in the PPC curve (Figure 1A). *Relative* volume changes (Figure 1D) are quantified in terms of the coefficient of the isobaric volume expansion, α:

$$\alpha \equiv \frac{\partial V_S}{V_S \partial T}\bigg|_p \qquad (1)$$

Considering, for instance, the values at 60 °C, it turns out that the larger absolute expansion of TM compared to LM arises simply from the larger size of TM; the relative expansion is ~0.8‰/K in both cases. MM, however, shows also a somewhat higher α(60 °C), which could be interpreted in terms of a larger contribution to α of the tail compared to that of the headgroup.

Figure 2A illustrates that the micellar transition becomes broader and is shifted to higher temperature upon dilution from 300 to 10 mM. Each data point shown for 10 mM MM is the average of the results obtained after 8 pressure jumps (4 up and 4 down). When the uncertainty in defining a baseline is taken into account, particularly for the 10 mM curve, there is no significant change in ΔV_S as a function of concentration. Exchange of H_2O by D_2O promotes the formation of rods, as indicated by a downshift in the transition temperature by ~4 K (cf. Figure 2C and data for 37 mM TM and MM in Table 1). The evaluation of the curve in D_2O was based on the reference-specific volume of 0.83 mL/g as in H_2O (cf. Experimental Section in the Supporting Information); the uncertainty of this value leads to an increased error of the absolute values of $\partial V_S/\partial T$ but does not affect the result for the transition volume, ΔV_S, substantially, which shows no significant deviation from the corresponding values in H_2O.

DSC. Figure 3 shows DSC curves of 37 mM MM in H_2O and D_2O. The transitions are endothermic, like all equilibrium

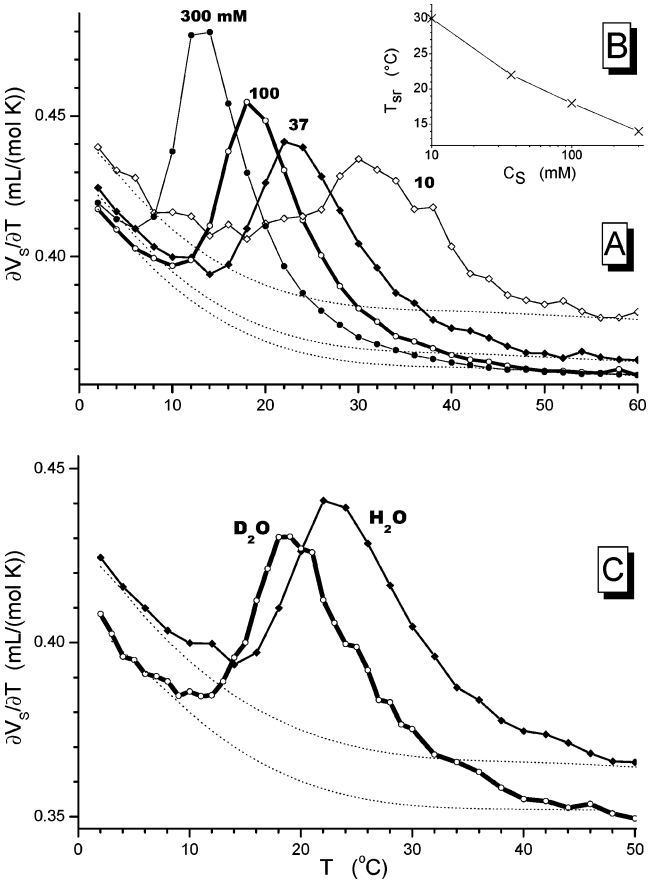

Figure 2. PPC curves of dispersions of MM as a function of concentration (A and B) and H_2O/D_2O substitution (C). (A) Experiments in H_2O at concentrations given in the plot. The inset in B shows the decrease in transition temperature, T_{sr}, as a function of the concentration on a semilogarithmic scale. (C) PPC curves of dispersions of 37 mM MM in H_2O and D_2O.

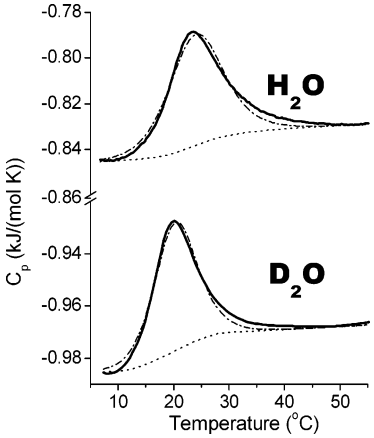

Figure 3. Raw DSC curves of 37 mM micellar dispersions of MM in H_2O and D_2O (bold solid lines) and the progress baselines (dotted) used for integration to derive ΔH (see Table 1). The curves were fitted by a model (dash−dot lines) based on a two-state transition of a single type of cooperative unit.

transitions driven by increasing temperature. The absolute values of the apparent C_p are not corrected for the heat capacity of excess H_2O/D_2O in the reference cell and, therefore, are not straightforward to interpret. The arbitrary assignment of progress baselines (cf. dotted curves in Figure 3) makes it possible to integrate the DSC peaks (yielding the enthalpy of the transition) and to estimate the step-height between the baselines extrapo-

lated from below and above the transition, which corresponds to the molar heat capacity change of the transition, ΔC_p. It seems to be slightly positive (0.010 ± 0.005 J/mol K), but the very small value and the uncertainty of the baseline hinder a precise determination. For a two-state transition, the width and shape of the peaks are determined by the van't Hoff enthalpy change, ΔH_{vH}.[35,36] It describes the same process as the calorimetric enthalpy change, ΔH (corresponding to the area underneath the peak), but is normalized per mole of cooperative units (c.u.) rather than per mole of monomers (as for ΔH). The size of a cooperative unit, c.u., is the number of monomers that undergoes the transition as a single unit. We obtained satisfactory fits assuming a single type of cooperative units (cf. dash−dot lines in Figure 3) with van't Hoff enthalpies of 220 and 280 kJ/mol c.u. for H_2O and D_2O, respectively, yielding c.u. $= \Delta H_{vH}/\Delta H \approx 300$ and 600. Other c.u. values are included in Table 1. Consistent with the PPC curve, the transition is shifted to lower T_{sr} and narrowed (larger c.u.) in D_2O compared to that in H_2O, and the enthalpy change, ΔH, is slightly smaller.

Comparison of the volume and enthalpy changes accompanying a transition allows one to estimate the dependence of the transition temperature, T_{sr}, on pressure, p, according to

$$\frac{\partial T_{sr}}{\partial p} = -T_{sr}\frac{\Delta V_S}{\Delta H} \qquad (2)$$

as derived from the Clausius−Clapeyron equation[6,37,38] (note that 1 mL/kJ converts into 1/10 kbar). The DSC curves recorded for TM and MM at different concentrations and in H_2O and D_2O correspond to a common pressure dependence of 50 ± 5 K/kbar, and $C_{14}EO_7$ in H_2O yields a significantly smaller value of 11 K/kbar.

It is noteworthy that PPC and DSC transition peaks (after baseline subtraction) have virtually the same shape (not explicitly shown). This is a consequence of the fact that the changes in volume and enthalpy occurring during the transition are coupled. The same observation was made for chain melting transitions of phospholipids[6,39,40] and explained theoretically.[39] The identity of the shapes makes it also possible to determine ΔH_{vH} from the PPC curves. Independent evaluations of the shape of the relatively pronounced PPC and DSC peaks of MM and $C_{14}EO_7$ yielded fairly consistent results. A comparison of PPC and DSC curves is particularly useful for the broad peaks of TM where the uncertainty in assigning a baseline limits the precision of the data evaluation.

DLS. Figure 4 shows the progress of the sphere-to-rod transition as obtained from DLS and integration of the PPC curve, both indicating a micellar transition of MM at about 20 °C, but only a much weaker thermotropic growth of TM micelles (at higher temperature) and hardly any significant growth of LM micelles.

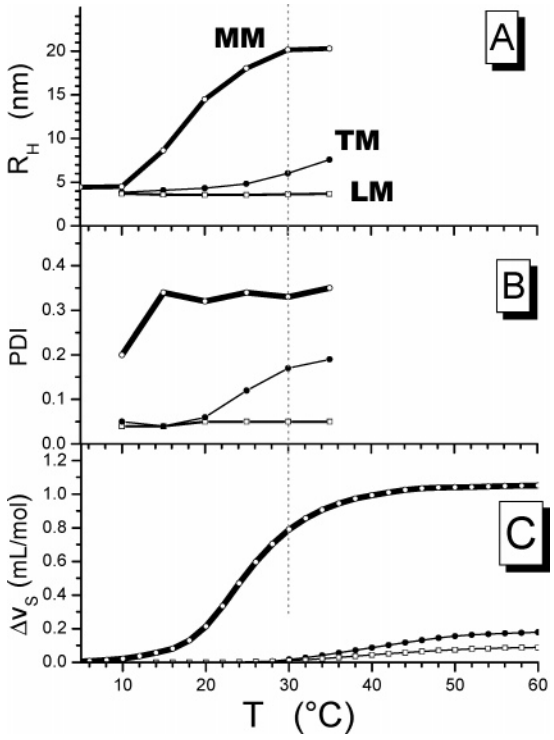

Figure 4. Progress of the sphere-to-rod transition of MM, TM, and LM (as labeled in panel A, all 37 mM) as reflected by the increase in the hydrodynamic radius, R_H, (A) and polydispersity index (B) measured by dynamic light scattering (DLS) and the volume change (integrated PPC curve after baseline subtraction, panel C). The maximum error of R_H is ±3 nm.

The DLS data of MM at 5 °C provide good evidence for an essentially spherical geometry. The fact that the hydrodynamic radius, R_H, of about 4.5 nm is somewhat larger than the maximum projected length of a surfactant molecule (~3 nm) can be explained by bound water contributing to R_H, the roughness of the micellar surface, and perhaps minor deviations from an ideally spherical shape. This is in line with the polydispersity index (PDI) of ~0.2, indicating only minor deviations from a monodisperse sample. With increasing temperature, DLS reveals a growth and shape transition of the micelles. R_H increases strongly to about 20 nm at 35 °C, which cannot be realized by spherical micelles since the molecules are only ~3 nm "long". The intensity distribution in the transition range (not shown here) shows two populations with different form factors, which is indicative of a coexistence of different shapes (in varying proportions) rather than a gradual elongation of the spheres. This polydispersity is also reflected by the large PDI.

TM shows a much weaker but significant increase of R_H (from 4 to 7 nm) and the PDI, showing a slight increase in the average size and polydispersity at about 25 °C.

LM micelles form a fairly monodisperse population (PDI ≪ 0.1) of spherical micelles of $R_H \approx 3.5-4$ nm (effective length of LM ≈ 2.6 nm) over the whole temperature range that is accessible to our DLS instrument. PPC suggests that a slight growth might take place at higher temperatures, but the effect is extremely weak and its significance is questionable.

For comparison, panel C of Figure 4 shows the transition curves obtained by integrating the PPC peaks after subtraction of the baseline. Generally, a good agreement is observed with the DLS data. It should, however, be noted that the effective

(35) Leharne, S. A.; Chowdhry, B. Z. In *Biocalorimetry*; Chowdhry, B. Z., Ladbury, J. E., Eds.; John Wiley and Sons: Chichester, U.K., 1998; pp 157−182.
(36) Blandamer, M. J.; Briggs, B.; Brown, H. R.; Burgess, J.; Butt, M. D.; Cullis, P. M.; Engberts, J. *J. Chem. Soc., Faraday Trans.* **1992**, *88*, 979−984.
(37) Anthony, F. H.; Biltonen, R. L.; Freire, E. *Anal. Biochem.* **1981**, *116*, 161−167.
(38) Landwehr, A.; Winter, R. *Ber. Bunsen-Ges. Phys. Chem.* **1994**, *98*, 214−218.
(39) Ebel, H.; Grabitz, P.; Heimburg, T. *J. Phys. Chem. B* **2001**, *105*, 7353−7360.
(40) Heerklotz, H.; Szadkowska, H.; Anderson, T.; Seelig, J. *J. Mol. Biol.* **2003**, *329*, 793−799.

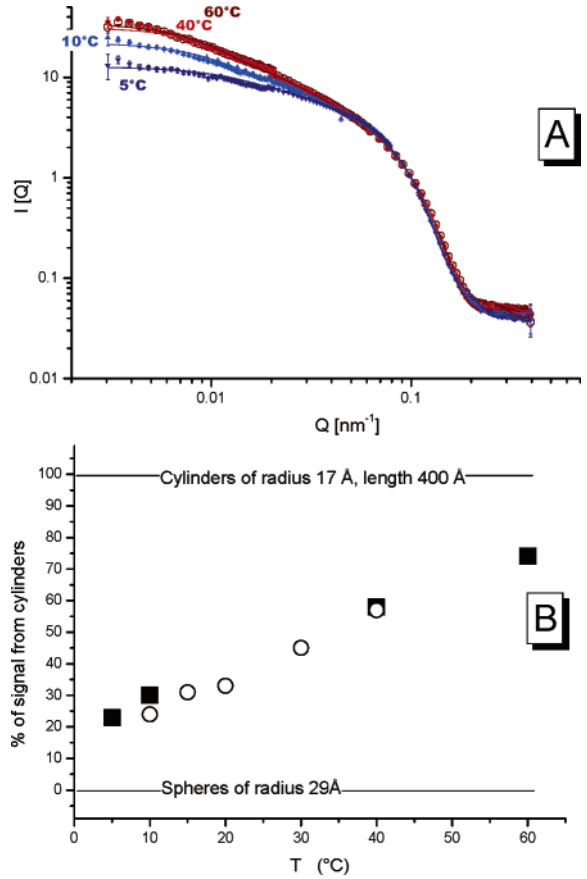

Figure 5. SANS data of 100 mM MM in D_2O at 60 °C (○), 40 °C (●), 10 °C (▲), and 5 °C (▼) and fit curves (A). The fits were based on a fixed scattering length density of $\eta = 1.048 \times 10^{-6}$ cm^{-2} and a fixed scaling factor of $\sigma = 0.1$ in the LogNorm distribution (see Experimental Section in the Supporting Information). All fits indicated a coexistence of spheres and cylinders with the same geometry ($R_S = 28.7 \pm 0.9$ Å, $R_C = 16.9 \pm 1.0$ Å, $L_C = 402 \pm 75$ Å; ranges are standard deviations) but varying proportions. The percentage of cylinders is illustrated by panel B for samples of 37 mM (○) and 100 mM (■).

value of R_H and the scattering intensity are not directly proportional to the number of molecules being localized in rods compared to that in spheres. This is essentially the case for progress curves obtained by integrating PPC or DSC curves.

SANS. The neutron scattering intensity, *I*, as a function of scattering vector, *Q* (Figure 5), shows a slope depending on the dimensionality of the system. The increasing negative slope at low *Q* ($Q < 0.07$ Å^{-1}) is indicative of a change from a zero-dimensional system (small spherical micelles) to a one-dimensional geometry (long thin cylinders).

A detailed model evaluation of the scattering curves implies that they can be described in terms of a *coexistence* of spherical and cylindrical particles of virtually temperature- and concentration-independent radii (standard deviations ≤1 Å) but with the fraction of cylinders increasing strongly with temperature (cf. Figure 5B).

The interpretation of the SANS model parameters has to take into account the limitations of the model. The dispersions might contain a great variety of particles: rough and dynamic spherical, ellipsoidal, peanut-shaped,[28] and longer, flexible, and possibly branched rodlike micelles. The model reduces this possible variety to two ideal, smooth geometries: spheres and stiff cylinders. However, the fact that this simple model yields a good fit of the scattering curves implies that the deviations from these ideal shapes are not pronounced and that a more complex, more realistic model with additional adjustable parameters is not warranted by the data. Nevertheless, it is obvious that the deviations of the micelles from the two ideal shapes must affect the fit parameters. One may speculate that the effective length of the quasi-cylindrical parts, L_C, is related to the persistence length rather than the total length of the flexible rods. The fact that the values obtained for L_C are about 20 times the radius R_C suggests that the curvature of the rods is relatively weak and the local geometry is indeed close to a cylinder. A sophisticated quantitative characterization of the flexibility of the rods of a mixture of similar compounds, alkylpolyglucosides, with hexanol has revealed a Kuhn length of ∼100−150 Å.[15] Deviations of the small particles from an ideal spherical geometry and those of the cylinders from an ideally circular cross-section are likely to give rise to an overestimation of the radii.

Second, the micelles do not have a homogeneous scattering length density, η. Instead, η decreases gradually from 6.3×10^{-6} cm^{-2} in bulk D_2O to $\eta \approx 0.1 \times 10^{-6}$ cm^{-2} in the core of the micelle (as in oil). The model distinguishes only between the background and "effective particles" with a pre-set, homogeneous η of 1.0×10^{-6} cm^{-2}. This operational definition of the particle boundaries includes not only hydrocarbon but also some water and headgroups.

These limitations of the model account for the fact that the effective radius of the spherical micelles, R_S, is larger than the maximum projected chain length (∼19 Å), which would not be realistic for the hydrophobic core of an ideal, smooth sphere. Note also that the fraction of the scattering arising from cylinders (Figure 5B) is not the fraction of all molecules that are residing within cylinders (Figure 4C).

Despite these issues, the SANS data clearly demonstrate that the transition of MM micelles at about 20 °C is a sphere-to-rod transition. The rods have a relatively long persistence length, and the effective radius is significantly smaller (∼$^2/_3$) than that of the spheres. With increasing temperature, the number of rods increases on the expense of spheres, but the geometric parameters of the two types of micelles remain virtually unchanged.

ITC. The concentration-dependent enthalpy changes of MM were measured using ITC at various temperatures (cf. Figure 6A) The micelles dissociate upon injection into the cell until the CMC is reached, giving rise to a quasi-sigmoidal curve with the point of inflection at the CMC.

In particular, ionic detergents have been found to show a three-step behavior forming spherical micelles at the CMC which then grow cooperatively to rodlike micelles at the "second CMC" at, for example, 3·CMC.[28,41] Such a pattern is not observed for the nonionic detergents studied here.

A plot of the enthalpies of micelle formation, ΔH^{mic}, of MM versus temperature yields a linear dependency (Figure 6B). The slope is the heat capacity change of micelle formation, $\Delta C_p^{mic} = -0.60$ kJ/mol K, which is a large negative value, as is typical for processes driven by the hydrophobic effect. The temperature at which the CMC is minimum corresponds to the point where ΔH^{mic} vanishes, that is, the point of intersection of the fit line with the abscissa, $T(\Delta H^{mic} = 0) = 19.5$ °C. The CMC at 25 °C amounts to 10 μM. Again, no significant deviations from

(41) Kubota, Y.; Kodama, M.; Miura, M. *Bull. Chem. Soc. Jpn.* **1973**, *46*, 100−103.

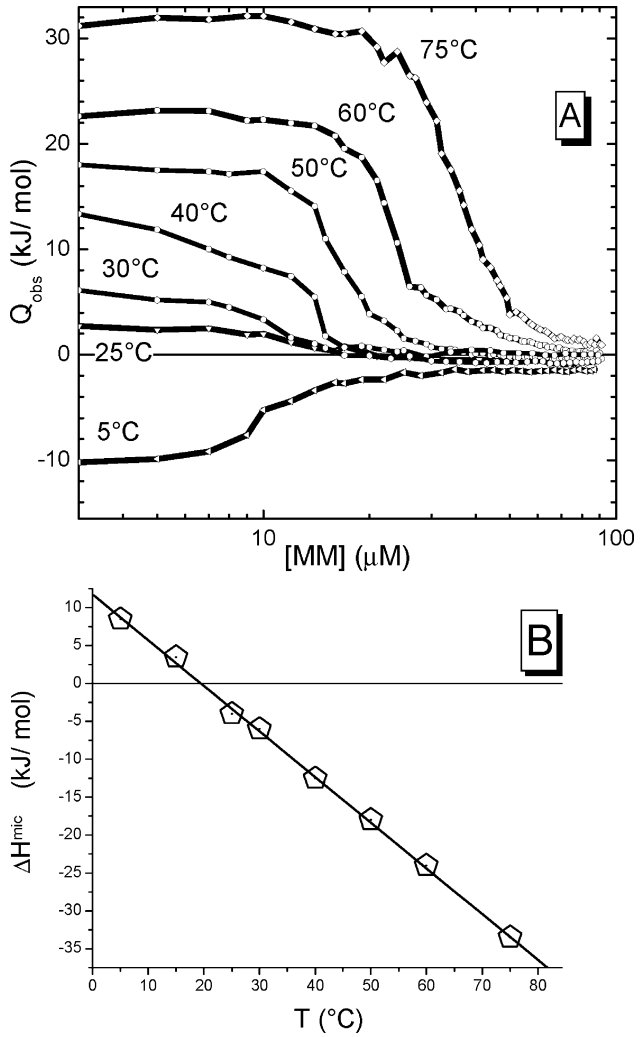

Figure 6. (A) ITC curves obtained upon demicellization experiments injecting micellar solutions of MM (0.5 mM) into water at different temperatures. (B) Enthalpies of micelle formation, ΔH^{mic}, as a function of temperature. The linear fit yields the heat capacity change, ΔC_p^{mic} (slope), and the temperature at the intercept with the abscissa, $T(\Delta H^{mic} = 0)$, where the CMC is minimum.

linearity are found that could be interpreted in terms of different structural states of the micelles at different temperatures.

For the micelle formation of TM, we obtained CMC(25 °C) = 35μM, $\Delta C_p^{mic} = -0.53$ kJ/mol K and $T(\Delta H^{mic} = 0) = 24$ °C; the results for $C_{14}EO_7$ are CMC(25 °C) = 7μM, $\Delta C_p^{mic} = -0.8$ kJ/mol K and $T(\Delta H^{mic} = 0) = 36$ °C.

Discussion

The various parameters of the sphere-to-rod transition determined here imply that the process is governed by a complex scheme of interrelated changes in headgroup hydration, ASA_{ap}, and chain order. An interpretation of the data requires all of these effects to be taken into account because each of the effects dominates some of the observable properties.

Headgroup Dehydration Triggers the Thermotropic Transition. A straightforward explanation why, for example, MM shows a thermotropic sphere-to-rod transition can be obtained in terms of the packing concept. Combination of Tanford's[42] empirical rules (cf. Materials) yields for the compounds studied here a virtually constant $v_{chain}/l_{max} \approx 21$ Å^2 so that the packing parameter becomes controlled exclusively by a_0, with a critical $a_0 \approx 60-65$ Å^2, corresponding to the transition between rods and spheres ($\gamma \approx 0.5$). A temperature-dependent variation of a_0 arises from a thermally activated dehydration of the headgroups, as shown for other nonionic surfactants, for example, using dielectric spectroscopy.[25,33] Kujawa and Winnik[4] characterized the thermal dehydration of a polymer in terms of a volume increase (~+1%) measured by PPC because water bound to polar groups has a larger density than does the characteristic hydrogen-bonded structure of bulk water (cf. also Chalikian[43]). The gradual, thermal dehydration of maltose in solution gives rise to a strong thermal volume expansion particularly below room temperature (Figure 1A). As expected, the sphere-to-rod transitions studied here are also accompanied by a positive ΔV_S, but the small absolute values suggest a partial compensation by other effects (changes in chain packing and ASA_{ap}).

It should be noted that in contrast to the sphere-to-rod transition, thermal dehydration is not a cooperative process that is initiated when a certain temperature is reached. No substantial peak of the PPC curve is found for maltose and LM, which show (virtually) no sphere-to-rod transition. That means that headgroup hydration inhibits the sphere-to-rod transition up to a certain temperature, that is, when it becomes too weak to overcompensate another force that promotes the transition. It is a temperature-dependent trigger but not the driving force of the transition.

The Chain Ordering Hypothesis. What cannot be understood in terms of the packing concept is why the tendency to form rodlike micelles decreases clearly with decreasing chain length. Although all long-chain alkyl maltosides share virtually the same packing parameter (cf. previous section), the tendency to form rods decreases from MM to TM and further to LM (Figure 1) and vanishes for octyl maltoside.[13] Furthermore, $C_{16}EO_8$ exhibits a T_{sr} lower than that of $C_{14}EO_8$[24], and the lyotropic micelle-to-hexagonal (i.e., rodlike) phase transition is promoted by longer chains comparing octyl, decyl, and lauryl maltoside.[44]

A key parameter of the alkyl chains that is not taken into account by the packing parameter is their degree of order, which is related to the average number of gauche defects. Molecules with a stronger propensity for a more ordered chain conformation will prefer micelle geometries inducing a higher degree of chain order and vice versa. However, the relationships between chain order and (i) chain length as well as (ii) spherical versus cylindrical geometry are not obvious.

(i) Unfortunately, there are no direct measurements of the order of methylene segments of different surfactants in micelles, but some clue of chain length effects on order can be derived from fluid phospholipid bilayers, which are well characterized by ^{2}H NMR.[45−47] Comparison of dilauroyl-, dimyristoyl-, and dipalmitoylphosphatidylcholine at a given temperature shows that the probability of a chosen C−C bond to form a gauche defect is higher for the longer chains,[47] suggesting that MM

(42) Tanford, C. *The Hydrophobic Effect: Formation of Micelles and Biological Membranes*, 2nd ed.; Wiley: New York, 1980.
(43) Chalikian, T. V. *J. Phys. Chem. B* **2001**, *105*, 12566−12578.
(44) Boyd, B. J.; Drummond, C. J.; Krodkiewska, I.; Grieser, F. *Langmuir* **2000**, *16*, 7359−7367.
(45) Seelig, A.; Seelig, J. *Biochemistry* **1974**, *13*, 4839−4845.
(46) Seelig, J. *Q. Rev. Biophys.* **1977**, *10*, 353−418.
(47) Douliez, J. P.; Leonard, A.; Dufourc, E. J. *Biophys. J.* **1995**, *68*, 1727−1739.

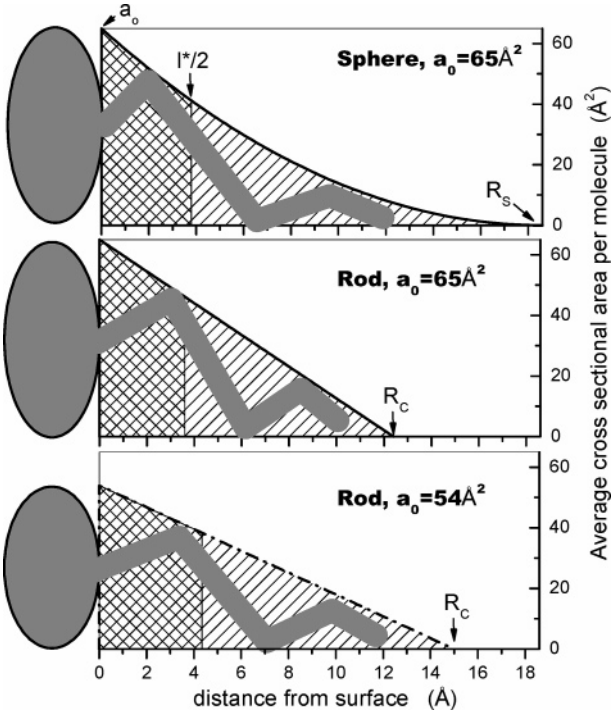

Figure 7. Mass distribution of a myristyl chain as function of distance from the surface in a sphere (top), in a cylinder with the same cross-sectional area at the interface ($a_0 = 65$ Å^2, middle), and a cylinder with a reduced interfacial area (54 Å^2, bottom). The intercept with the ordinate corresponds to the incremental surface area per molecule, a_0, and the area underneath the curves represents the incremental volume, $v_{chain} \approx 400$ Å^3, of a myristyl chain (outer 200 Å^3 crosshatched, inner 200 Å^3 hatched). The radius of the micelle core follows from the point where the curve reaches zero (midpoint of the micelle).

can be assumed to prefer a higher average degree of chain order than does LM.

(ii) Whether the effective order of the chains is higher or lower in a rodlike micelle compared to a sphere is also not straightforward to predict. A principal difference between spheres and rods is the area-to-volume ratio, amounting to $A/V = a_0/v_{chain} = 3/R_S$ for spheres and $A/V = a_0/v_{chain} = 2/R_C$ for cylinders. These two relations imply that for a sphere-to-rod transition, the radius should shrink to $R_C = 2R_S/3$ if a_0 and v_{chain} are conserved. Such a reduction of R, but to a somewhat lesser extent, was indeed observed in our study and measured[16] as well as theoretically predicted[28] in the literature. It is graphically illustrated in the top and middle panel of Figure 7, where the intercept with the ordinate corresponds to an arbitrarily chosen $a_0 = 65$ Å^2; the area under the curves (hatched + crosshatched) represents $v_{chain} = 400$ Å^3, and the points where the curves reach the abscissa are the corresponding radii, $R_S = 3v_{chain}/a_0 = 18.5$ Å and $R_C = 2v_{chain}/a_0 = 12.3$ Å.

The figure shows also that the distribution of mass (i.e., the volume increment of a thin shell) as a function of the distance from the surface follows a parabola for a sphere (which is curved in two dimensions) but a straight line for the cylinder. In contrast to the more homogeneous cylinder packing, the sphere must contain very few highly ordered/stretched chains with a projected length close to l_{max} but also a considerable number of highly disordered chains that fill the large volume fraction close to the surface (cf. also ref 28). On average, both systems seem to have similar degrees of order. As an indirect measure of chain order, let us define an effective projected chain length, l^*, so that half of the chain resides, on average, within a depth of $l^*/2$ from the surface. This value of $l^*/2$ is just the abscissa value which cuts the area under the curve in two halves (left crosshatched, right hatched in Figure 7). It is intriguing that $l^*/2$ (cf. Figure 7) and, in turn, l^* is very similar for the sphere ($l^* = 7.6$ Å) and the rod ($l^* = 7.2$ Å).

The bottom panel of Figure 7 illustrates the more realistic case that a_0 is smaller in the rod due to headgroup dehydration. Then, the radius is closer to that of the sphere, and the chain is more stretched. Already for a slightly dehydrated headgroup with $a_0 = 60$ Å^2, one obtains an $l^* = 7.8$ Å, which suggests a higher average order than in a sphere with $a_0 = 65$ Å^2.

Although a quantitative treatment in terms of the effect of changes in chain order on the free energy is not possible in the frame of our study, we conclude that there may well be a net stretching/ordering of the hydrocarbon chains accompanying the sphere-to-rod transition. Combined with the assumption that MM prefers an average chain order higher than that of LM, this would explain the findings of surfactants with longer chains showing a stronger tendency to form rodlike micelles.

The available information led us to the hypothesis that the sphere-to-rod transition increases the order of the chains, but we cannot rule out that a disordering (if MM would prefer less order than LM) or another parameter (not order) govern the chain length dependence of the transition. The hypothesis of increasing order accompanying the sphere-to-rod transition gives rise to the apparent paradox that increasing temperature promotes a process that reduces the entropy of the system. Such a chain ordering could neither account for driving nor for triggering the transition, but the phenomenon could be explained in terms of another "force", the hydrophobic effect, driving the transition and overcompensating the exothermic chain ordering enthalpy.

The Hydrophobic Effect Drives the Transition. A driving force for the sphere-to-rod transition arises from the coupling between the ideal geometrical surface area of the micellar core, a_0, and the water accessible apolar surface area (ASA_{ap}). Hence, the energy required for a reduction of a_0 by headgroup dehydration is provided by the hydrophobic effect favoring a small ASA_{ap}.

Good evidence for this reduction in ASA_{ap} is provided by our observation of a T_{sr} in D_2O that is lower than that in H_2O. Due to a more stable hydrogen-bond network, D_2O shows a stronger hydrophobic effect and promotes processes that are accompanied by a reduction in ASA_{ap}, such as micelle formation,[48,49] protein folding,[1,2,50] and the freezing of fluid lipids to a gel phase.[51] Micelle clustering was found to show a transition temperature higher in D_2O than in water.[36,52] We found no significant isotope effect on ΔV_S, which is similar to the freezing of lipid bilayers to a gel phase (cf. Wiener et al.[55]) but in contrast with the dehydration of polar groups upon protein folding and

(48) Kresheck, G. C. *J. Phys. Chem. B* **1998**, *102*, 6596−6600.
(49) Kresheck, G. C. *J. Am. Chem. Soc.* **1998**, *120*, 10964−10969.
(50) Hermans, J., Jr.; Scheraga, H. A. *Biochim. Biophys. Acta* **1959**, *36*, 534−535.
(51) Lipka, G.; Chowdhry, B. Z.; Sturtevant, J. M. *J. Phys. Chem.* **1984**, *88*, 5401−5406.
(52) Blandamer, M. J.; Briggs, B.; Burgess, J.; Cullis, P. M.; Eaton, G. *J. Chem. Soc., Faraday Trans.* **1991**, *87*, 1169−1175.
(53) Likhodi, O.; Chalikian, T. V. *J. Am. Chem. Soc.* **1999**, *121*, 1156−1163.
(54) Likhodi, O.; Chalikian, T. V. *J. Am. Chem. Soc.* **2000**, *122*, 7860−7868.
(55) Wiener, M. C.; Tristram-Nagle, S.; Wilkinson, D. A.; Campbell, L. E.; Nagle, J. F. *Biochim. Biophys. Acta* **1988**, *938*, 135−142.

the polymer globule formation.[4,53,54] Both the sphere-to-rod transition and lipid freezing involve coupled changes in chain order, ASA_{ap}, and headgroup hydration, which may have compensating isotope effects.

The reduction in ASA_{ap} explains why a sphere-to-rod transition can occur spontaneously, but it does not control whether it occurs and at which temperature. One might speculate that the transition is initiated when the hydrophobic effect reaches a certain, critical strength, but this idea is ruled out by the observation that increasing temperature drives the transition of TM at $T_{sr} \approx 30$ °C, where the driving force for hydrophobic association decreases (minimum of CMC is at 24 °C). Empirical rules for proteins given by Murphy[56,57] suggest that the reduction in ASA_{ap} could also account for the *endothermic* enthalpy change, whereas the gradual dehydration of the polar headgroups and an ordering of the chains should be exothermic.

Sphere-Rod Coexistence. On the basis of the most simple model describing a rodlike micelle as a cylinder with spherical end caps, one might expect that the sphere-to-rod transition is a continuous process since a gradual variation of the total length, L_C, can describe a transformation of a sphere (formally, $L_C = 2R_C$; i.e., the end caps touch each other) to a rod ($L_C > 2R_C$). Such a micelle could assume all aggregation numbers equal or larger than about 70 (corresponding to an ideal sphere formed by myristyl chains).

Our data provide strong evidence that this scenario is wrong (at least for the compounds studied here). DLS and SANS report a two-state transition between two distinct, coexisting geometries, which are spheres and rods of a minimum length, $L_C \geq 20R_C$ (SANS for MM). This is in line with the information from the van't Hoff enthalpy of the transition (DSC of MM, TM) that the formation of a stable rod requires the concerted association of 300−600 molecules (i.e., about 4−8 spherical micelles).

The energetic barrier which inhibits the formation of very short rods can be explained in terms of the different equilibrium radii of rods, R_C, and spheres (and spherical end caps, R_S). Such a barrier was indeed predicted by May and Ben Shaul[28] who calculated the interfacial bending energy of a peanut-shaped micelle with quasi-spherical end caps connected by a thinner, cylindrical part. They showed that the cylindrical part must have a minimum length to avoid strongly unfavorable interferences between the ends. One may wonder whether the smaller cooperative unit of rod formation by $C_{14}EO_7$ can be explained in terms of a different bending modulus of the micellar interface or other headgroup properties.

Effects of Concentration, Transition Temperature, and Pressure. The fact that the sphere-to-rod transition is promoted (i.e., T_{sr} is lowered) *with increasing surfactant concentration* (cf. Figure 1) follows the rule arising from the mass-action law that an increase in concentration promotes association or growth. At a lower concentration, the transition proceeds at higher temperature, T_{sr}, and less cooperatively (smaller c.u.), but the accompanying volume change remains virtually constant. This observation is important because it provides some insight into the temperature dependence of ΔV_S and ΔT_{sr}. In contrast to the micellar shape transition studied here, the temperature of micelle clustering increases with increasing temperature.[36,52] The concentration dependence of T_{sr} implies also the existence of a concentration-driven sphere-to-rod transition, but this turns out to be very gradual. Figure 2A shows that, for example, at 20 °C, the transition to rods starts at ∼10 mM and is largely completed at 300 mM. When this is taken into account and the fact that ΔH is small compared to the enthalpy of demicellization, it becomes clear why there is no "second CMC" for MM which could be detected by ITC.

It is the nature of the transition studied here that the number of rods increases at the expense of spheres with increasing *temperature*. The structural parameters of the spheres and rods as well as the volume and enthalpy changes accompanying the sphere-to-rod transition are, however, virtually independent of T_{sr}. In agreement with this fact, ΔC_p and $\Delta\alpha$ are small, and ΔC_p^{mic} is virtually independent of T.

The effect of *elevated pressure* on the sphere-to-rod transition temperature, $\partial T_{sr}/\partial p$, can be assessed on the basis of the DSC and PPC data (ΔH, T_{sr}, and ΔV_S). Since the sphere-to-rod transition increases the volume, it is opposed by enhanced pressure. The effect is relatively strong for MM and TM (∼50 K/kbar) but weaker for $C_{14}EO_7$ (∼10 K/kbar). Values of ∼40 K/kbar were reported for the lamellar-to-inverse hexagonal transition of lipids, which is also accompanied by a change in interfacial curvature and tighter packing of the headgroups.[38] The pressure dependence of phospholipid melting is somewhat weaker (∼20 K/kbar).[38,58] It is interesting to note that this parameter seems to be conserved for the melting of phospholipids with saturated chains irrespective of chain length and headgroup, despite major differences in ΔH, ΔV, and T_m. This can be considered as a clue that this pressure dependence is a characteristic property of trans-gauche isomerization of the chains. In contrast, the sphere-to-rod transitions and the Krafft points[59] of different surfactants do not obey a common pressure dependence.

Conclusions

It was shown that a combined thermodynamic, volumetric, and structural approach can provide a new level of understanding of a phenomenon, such as the sphere-to-rod transition. Volumetric data could be obtained very precisely and conveniently using PPC. This study gives rise to the following conclusions:

(1) The thermotropic sphere-to-rod transition is driven by a reduction in the water accessible apolar surface area, ASA_{ap}, which is favored by the hydrophobic effect. This is indicated by a downshift of the transition temperature in D_2O compared to H_2O and may account for the endothermic enthalpy change.

(2) The transition is triggered by a weaker hydration of the surfactant at higher temperature, which allows the hydrophobic effect to reduce the interfacial area per molecule. Like other phenomena of polar group dehydration, the sphere-to-rod transition is accompanied by an increase of the partial volume.

(3) The characteristic chain length dependence of the thermotropic sphere-to-rod transition gives rise to the hypothesis that the sphere-to-rod transition is accompanied by an ordering of the alkyl chains; that is, chains in a cylindrical aggregate pack more favorably than in a sphere.

(56) Baker, B. M.; Murphy, K. P. *Methods Enzymol.* **1998**, *295*, 294−314.
(57) Murphy, K. P. *Med. Res. Rev.* **1999**, *19*, 333−339.
(58) Prasad, S. K.; Chandrasekhar, S.; Shashidhar, R.; Gaber, B. P. *Biophys. J.* **1990**, *57*, A557.
(59) Kaneshina, S.; Yamanaka, M. *J. Colloid Interface Sci.* **1990**, *140*, 474−480.

(4) The nonionic surfactants studied here show a concentration-dependent micellar structure but not as a cooperative phenomenon like a "second CMC".

(5) The sphere-to-rod transition is opposed by increasing pressure with a shift of the transition temperature by ~50 K/kbar for MM and TM, but this value does not seem to characterize all sphere-to-rod transitions.

Acknowledgment. We are indebted to Halina Szadkowska for excellent technical assistance, and to Joachim Kohlbrecher for providing the sasfit program. We thank a reviewer for suggesting a van't Hoff analysis of the DSC peaks. Financial support from the Swiss National Science Foundation is gratefully acknowledged by H.H. and A.T. (Grant 31-67216.01). Part of this work was performed at SINQ, Paul Scherrer Institute, Villigen, Switzerland.

Supporting Information Available: Experimental details in the Experimental Section. This material is available free of charge via the Internet at http://pubs.acs.org.

JA045525W